Solar Energy Materials & Solar Cells 143 (2015) 529–538

Contents lists available at ScienceDirect

Solar Energy Materials & Solar Cells

journal homepage: www.elsevier.com/locate/solmat

Degradation of transparent conductive oxides: Interfacial engineering and mechanistic insights

Heather M. Mirletz [a,b,c,1], Kelly A. Peterson [a,c,e], Ina T. Martin [b,d,c], Roger H. French [a,c,d,*]

[a] Solar Durability and Lifetime Extension (SDLE) Center, Case Western Reserve University, Cleveland, OH 44106, United States
[b] Materials for Opto/Electronics Research and Education (MORE) Center, Case Western Reserve University, Cleveland, OH 44106, United States
[c] Department of Materials Science and Engineering, Case Western Reserve University, Cleveland, OH 44106, United States
[d] Department of Physics, Case Western Reserve University, Cleveland, OH 44106, United States
[e] Department of Chemistry, Case Western Reserve University, Cleveland, OH 44106, United States

ARTICLE INFO

Article history:
Received 13 February 2015
Received in revised form
14 July 2015
Accepted 18 July 2015

Keywords:
Transparent conductive oxide
Degradation science
Organic photovoltaics (OPV)
Interfacial properties
PEDOT:PSS
Silane

ABSTRACT

Transparent conductive oxides (TCOs) are a known failure mode in a variety of thin film photovoltaic (PV) devices, through mechanisms such as resistivity increase and delamination. Degradation science studies of these materials, as well as most PV systems, have primarily utilized industry standard qualification protocols, which are not designed to be used as lifetime prediction tests. This work applies a data science approach to this engineering challenge, utilizing commercially available TCOs and subjecting them to an array of stressors, including environmental and material stressors. Optical, electrical and surface sensitive TCO property metrics were monitored and analyzed en mass. Different degradation mechanisms and modes were observed when different stressor combinations were applied; TCO surfaces are sensitive to the proportion of water and light in an exposure, yellowing of the TCO only occurs when humidity and UV light are combined, and PEDOT:PSS (poly(3,4-ethylenedioxythiophene) poly(styrenesulfonate)) application results in hazing and roughening of aluminum-doped zinc oxide (AZO). Using multi-variate analytics and plotting critical material properties against one another in a mechanistic plot, trade-offs between properties and the activation of different degradation mechanisms become readily apparent. In addition to a survey of failure modes of TCOs, a possible solution to the degradation of AZO was examined: the application of an organofunctional silane layer. The application of a thin APTES (3-aminopropyltriethoxysilane) film nearly eliminated the observed edge effects and greatly reduced the resistivity increase caused by damp heat exposure of AZO.

1. Introduction

The transparent electrode is a constituent of numerous optoelectronic devices, including photovoltaic (PV) devices, display and touch screens, and organic light emitting diodes (OLEDs). A variety of materials are used as transparent electrodes; active areas of research include transparent conductive oxides (TCOs), conductive polymers, such as PEDOT:PSS [1,2], and nanowire networks, such as silver nanowires [3,4]. The device context and expected lifetime of the application determine material durability requirements. PV is a long-lifetime application that involves a myriad of environmental stressors; TCOs are widely used as transparent electrodes in PV, and TCO degradation is a critical failure mode in many PV technologies [5–8]. Delamination at the TCO-absorber and TCO-glass interfaces has been reported in thin film silicon [9–11], copper indium gallium selenide (CIGS) [7,12,13], and organic PV (OPV) technologies [14–17]. Interfacial degradation is often an avenue for delamination and device failure, and control of interfaces is important to device performance [11,17–19]. Additionally, voltage-biased electrochemical corrosion of the TCO can lead to cracking [9,10,20], and increased resistivity and structural changes (including roughening and pitting) are widely observed in a number of optoelectronic devices [7,21–23,12].

In optoelectronic applications, TCO surfaces are often modified with one or more thin interfacial layers (IFLs), such as polymers, organofunctional silanes, and small molecule adsorbates [11,17,24–27]. These modifications are designed to improve device performance by controlling the TCO work function, optimizing rates of charge-carrier transfer, and increasing the compatibility of the polar TCO with nonpolar materials used in OPVs and OLEDs.

Although IFLs can enhance initial device performance, the effect of the IFL on the device's lifetime performance must also be

* Corresponding author at: Department of Materials Science and Engineering, Case Western Reserve University, Cleveland, OH 44106, United States. Tel.: +1 216 368 3655.
E-mail address: roger.french@case.edu (R.H. French).
[1] previously Lemire.

http://dx.doi.org/10.1016/j.solmat.2015.07.030
0927-0248/

considered. PEDOT:PSS (poly(3,4-ethylenedioxythiophene) poly (styrenesulfonate)) is a polymer commonly used as an electron blocking layer in OLEDs and standard architecture OPV devices to improve device efficiency and adhesion between the ITO (indium tin oxide) TCO and the polymer absorber layer [17]. However, PEDOT:PSS is highly acidic and hygroscopic, causing corrosion of the TCO layer (via dissolution of the indium from the In_2O_3 matrix) [15–17,28] and water-related damage to the entire device [8,29]. Other commonly used IFLs are organofunctional silanes; these have been used for decades as coupling agents between organic materials and inorganic surfaces, including in OPV and OLED devices to improve performance [30,31,19]. Silanes are an excellent candidate for interfacial layers in PV devices due to their dipole-like structure, their customizability, and their established use in commercial processes [24,32,33]. With respect to OLED device stability, incorporating a silane interlayer at the ITO/PEDOT:PSS interface has been shown to block the detrimental interaction between PEDOT:PSS and ITO over a short time frame [14].

For lifetime and degradation science (L&DS), the ideal outcome of an accelerated exposure is to provide rapid, straightforward insights into the lifetime performance of a material or device [34–37]. In an L&DS study, normal experimental approaches are complemented with an epidemiological approach using data science and statistical analytics. Materials, samples, and devices are considered as a system, and responses under applied stress are observed using a stress and response framework perspective [34]. All exposure conditions (stressors) and all experimentally measured properties are considered variables, and methods of exploratory data analysis (EDA) are used to identify relationships among variables. This data science approach complements the traditional hypothesis driven approach; new, statistically significant degradation modes and mechanisms can be uncovered by the addition of EDA, and detailed statistical analysis of the variables can provide confirmatory insights [38]. From these data, the next step in L&DS can be taken: developing predictive (prognostic) models demonstrating the observed relationships, enabling exploration of the materials and device performance for real world application [39,40]. Mechanistic degradation models, semi-gSEM (semi-supervised by domain science, generalized Structural Equation Models) can be developed to capture the system's response to stressors [35,41]. Here, the first steps in an L&DS study are conducted on TCOs.

Current industry standard tests were developed as qualification standards for safety marketability, not as lifetime predictors, generating a need for L&DS. Recent studies and colloquial knowledge have questioned whether these industry standard exposures are accurate predictors of real world degradation mechanisms [5,42,43]. Whereas degradation studies of TCOs and TCO devices have been conducted, most have focused on various forms of damp heat testing [9–11,7,21–23,12,44]. The present study broadens the literature, showing that comparison of multiple stressor combinations, including environmental and situational stressors, is necessary to provide insight into degradation mechanisms, including enabling comparison and cross-correlation of performance under accelerated and real world conditions.

In this study, a L&DS approach is applied to the engineering challenge of TCO degradation; illumination, humidity and temperature stressors are applied in various combinations to commercially available TCOs, exploring encapsulation, a polymer stressor (PEDOT:PSS), and a proposed protective silane interfacial layer (3-aminopropyltriethoxysilane, APTES). The optical, surface, and electrical properties of the TCOs were monitored, yielding insights into mechanisms of TCO degradation.

2. Experimental procedures

AZO (Zhuhai Kaivo Electronic Components Co., Ltd.), ITO (Colorado Concept Coatings LLC), and FTO (Hartford Glass Company Inc.) on soda lime glass (5 cm by 5 cm) were purchased commercially. Samples were subjected to exposures in 168 or 336 h (1 or 2 week) increments (steps) for a total of 1000 to 2526 h of exposure, and samples were removed at 6 time increments during the exposure. After each exposure step, 2–3 samples were removed, cleaned, and characterized. All samples were saved after exposure as part of a retained sample library for further studies. Samples were exposed in one of 4 configurations; open-faced, edge seal encapsulated, edge seal encapsulated with PEDOT:PSS, or open-faced with silane.

Averaged data are shown in the results section and, where applicable, a *t*-test was performed on the raw data to confirm statistically significant difference [45]. The optical and electrical properties of FTO were found to be robust under all exposure conditions used in this study (open faced accelerated), an observation consistent with the literature [21,46]. ITO was also statistically robust for many of the monitored exposure conditions and evaluation variables. A total of 234 samples were exposed; the subsets showcased in the results and discussion are shown in Fig. 1 [38].

This study is done in the spirit of open [47–50] and reproducible science [47,51,52]. Data were analyzed using open source software, the R programming language [53–56]. All data and the R analysis code to reproduce these analyses are available under an open data license at https://hml15@bitbucket.org/vuvlab/13odlemiretcos.git [57].

2.1. Measurements of TCO properties

All samples were cleaned before and immediately after exposure to remove any environmental test chamber contaminants before data collection [58]. Sample cleaning involved a series of 10 min sonications in 30 °C solvents (acetone, isopropanol, DI water), drying under nitrogen gas, and a 15 min UV ozone clean at 60 °C (Novascan PSDP-UV8T). Contact angle data were collected first to minimize time-dependent surface contamination in room air conditions. Then optical measurements were taken, followed by the resistivity measurements.

Contact angle values were collected by taking the averages of 50-frame video measurements at 5 locations on 2 samples (5 water videos from one sample, 5 diiodomethane videos from the other sample). Transmission spectra were obtained using an

Study Sample Map

		Bare TCO		PEDOT:PSS		Silane	
		AZO	ITO	AZO	ITO	AZO	ITO
Open Faced	Hot QUV	12	12				
	Damp Heat	12	12			12	12
	Cyclic	18	18				
Encapsulated	Damp Heat	6	6	12	12		
	1x Outdoor	6	6	12	12		
	5x Outdoor	6	6	12	12		

*encapsulated TCOs without PEDOT:PSS were removed from exposure in pairs at exposure steps 1, 3, and 6.

Fig. 1. Matrix showing the number of samples, exposure type and exposed sample configuration. Samples were removed, tested, and stored in a retained sample library at 6 time increments throughout the exposure duration.

Agilent Cary 6000i, inline transmission, equipped with a DRA-1800 integrating sphere. Percent haze, yellowness index (YI), L^*, a^*, and b^* values, were obtained using a Hunterlab UltraScan Pro Colorimeter; L^* is the perpendicular axis tracking white to black, and a^* and b^* are the axes of the color plane. L^*, a^*, and b^* are used to calculate YI and percent haze. Changes in L^*, a^*, and b^* are not necessarily detrimental, but increases in yellowness and % haze are generally taken to be negative as they reduce the amount of light reaching the absorber; yellowness is a surface sensitive measurement that can show degradation before a transmission spectrum would. The resistivity of the ITO films were measured using an EDTM R-chek (model# RC2175) four point probe (edge effect deviations of up to 20% were corrected for in accordance with manual guidelines), and the resistivity of the AZO films were measured using a Keithley 2400 Source and Lucas Labs four point probe, which penetrates slightly into the film. The resistivity measured in the center of the 5 × 5 cm square samples is reported. Microscope images were collected with a Leica DM 2500 M microscope at 5 × magnification to observe edge effects of AZO.

2.2. Exposure parameters

Five exposure protocols were used (3 accelerated and 2 real world): ASTMG154 X2.1-Cycle 4 (cyclic), Modified ASTMG154 X2.1-Cycle 4 (5 suns UV), IEC 61626 (damp heat, DH), and outdoor exposures at 1 × and 5 × concentrations on a dual-axis tracker (see Table 1). Note that ASTMG154 X2.1-Cycle 4 is one of the commonly used set of irradiance settings; in this case, the irradiance that is approximately equivalent to 5 suns of UV light at 340 nm [59]. The 5 × outdoor exposure used front surface aluminized hexagonal mirror concentrators to concentrate the sunlight, such that the final irradiance is 5 times the sun's direct irradiance.

2.3. Encapsulation

Encapsulation serves to prevent water condensation on the materials of interest while not hampering the diffusion of humidity into the system [60]. Samples were prepared for encapsulation by wet etching the ITO and AZO samples with 50:50 concentrated HCl:H_2O solution to remove the edges, cleaning, applying 1/3 of a 10 mm width of Quanex Solargain™ Edge Tape – SET LP03 (WVTR 0.3 g/m^2/day at 100% Relative Humidity (RH), 37.8 °C) on each etched edge, and placing a 5 cm by 5 cm glass square on top of the edge tape. Glass-glass lamination was accomplished in a P.Energy L036LAB panel laminator at 90 °C and 500 mPa after 10 min evacuation. The samples were delaminated by dipping the samples in liquid nitrogen.

2.4. PEDOT:PSS

For samples aged with OLED-grade PEDOT:PSS, the as-received polymer from Clevios (PVP AI4083, resistivity of 750 Ω cm, solids 1.75%) was spun cast onto the etched, cleaned TCO before lamination. The polymer was spun at 4000 rpm for 40 s and post-baked for 10 min at 150 °C. The PEDOT:PSS was wiped from the edges of the glass with a DI water dampened optical wipe. Samples were stored in nitrogen until encapsulation, with less than 10 min of air exposure after PEDOT:PSS deposition. Post-exposure, the PEDOT:PSS was removed with a DI water-dampened optical wipe, and the TCO was solvent cleaned before data collection. All PEDOT:PSS related data presented are taken on the TCO after the PEDOT:PSS was removed, unless otherwise stated.

2.5. Silanization

APTES films were deposited on clean TCO samples in a 1% v/v silane/anhydrous toluene solution for 60 min at 65 °C, followed by a series of solvent rinses (anhydrous toluene, chloroform, methanol), drying under nitrogen, and a 10 min bake at 120 °C. As a trifunctional silane, APTES (shown in Fig. 2) can create up to 3 bonds with surfaces or other APTES molecules, forming multi-layers [61,30]. Conditions were chosen to form a thin (approx. 1 nm), continuous film on the TCO surface [30]. Baseline contact angle measurements of the TCO+silane stack were acquired on freshly deposited samples.

After exposure, the TCO+silane stack was solvent cleaned, and the APTES layer was removed with a 40 min UV-ozone clean at 60 °C. Silane removal was confirmed using water contact angle measurements before proceeding with TCO cleaning and data collection. All data presented for silanized TCOs are taken on the TCO after the silane was removed, unless otherwise stated.

3. Results

3.1. Open-faced TCO degradation

Three transmission spectra of AZO in various exposures and configurations are compared to their baselines in Fig. 3, providing a qualitative survey of the degradation modes. Fig. 3 shows AZO after ~1000 h of (a) 5 suns UV exposure, (b) damp heat exposure, and (c) cyclic exposure. Different features appear in the post-exposure spectra for each stressor combination; no degradation is apparent in the 5 suns UV exposure (light stressor). After damp heat exposure (humidity stressor), a peak-trough height reduction is observed, which suggests surface roughening. Cyclic exposure,

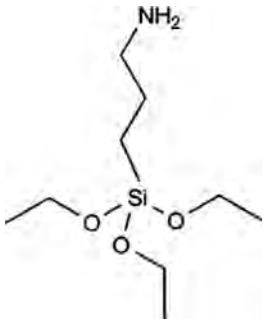

Fig. 2. Structural formula of APTES [61].

Table 1
Exposure parameters used in this study protocol.

Exposure name	Conditions	Equipment	Stressors
Modified ASTMG154 X2.1-Cycle 4, "5 suns UV"	70 °C and 1.55 W/m^2/nm @ 340 nm	QUV Spray	Heat, UV light
IEC 61646.10.13, "damp heat," "DH"	85 °C, 85% relative humidity	CSZ ZPH8	Heat, Humidity
ASTMG154 X2.1-Cycle 4, "cyclic"	8 h @ 70 °C, 1.55 W/m^2/nm @ 340 nm, 4 h @ 50 °C with spray in dark	QUV Spray	Heat, UV light, Humidity
Outdoor 1 ×	Cleveland weather June–October	dual-axis tracker	"Heat", Sunlight, Humidity
Outdoor 5 ×	Cleveland weather June–October, front surface mirror concentrator	dual-axis tracker	"Heat", Sunlight, Humidity

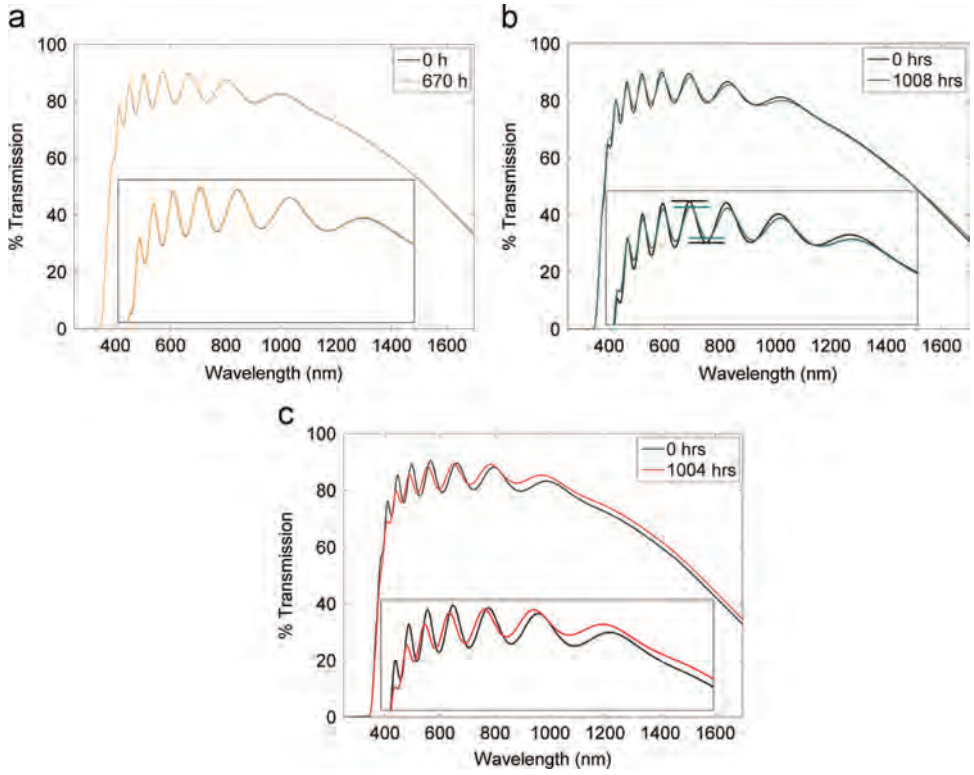

Fig. 3. The %transmission spectrum of AZO from 1800 nm to 200 nm, for (a) 5 suns UV, (b) damp heat, (c) and cyclic exposures, qualitatively demonstrating increasing degradation with additional stressors. The cyclic exposure, which combines water and light, shows the greatest degradation.

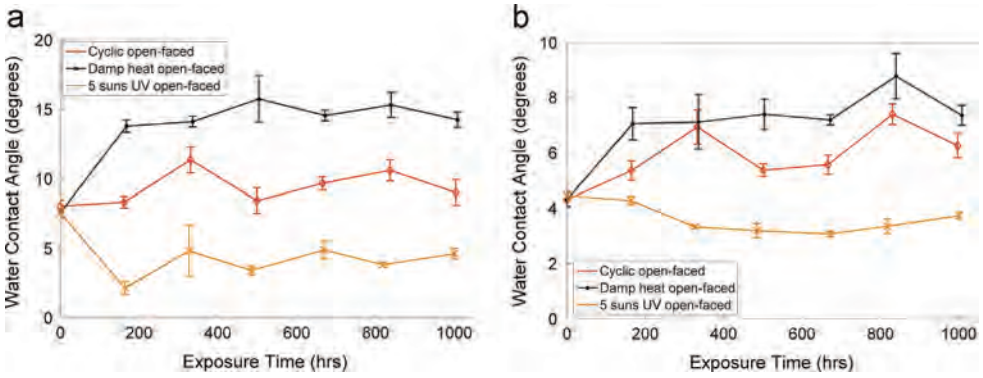

Fig. 4. Water contact angles of (a) AZO and (b) ITO in the three accelerated exposures, 5 suns UV, damp heat, and cyclic. The exposures are "ranked" in order of increasing water content in the exposure; 5 suns UV with the lowest water content and contact angle, damp heat with the highest, and cyclic in the middle.

which combines humidity and light stressors, results in not only a peak-trough height reduction, but also a rolling of the fringes, and an increase in transparency in the IR region. Rolling of the fringes suggests a change in film thickness, and the increase in transmission in the IR region is tied to a reduction in free carriers [12]. No changes were observed in the transmission spectra of ITO after 1000 h of the same three exposures.

To examine the degradation quantitatively in a statistically robustly fashion, we turn to a variety of metrics that produce discrete data. The effect of accelerated open-faced exposures on the water contact angles of AZO (a) and ITO (b) surfaces are shown in Fig. 4. It is observed that the contact angle scales with the water content of the exposure: 5 suns UV with no active addition of water results in a lower water contact angle, damp heat at 85% relative humidity results in a higher water contact angle. The cyclic exposure, alternating water spray and the 5 suns UV parameters, maintains the initial, unexposed water contact angle.

Neither the damp heat nor the 5 suns UV exposure resulted in a change in AZO YI, Fig. 5. However, the AZO YI does increase in the open-faced cyclic exposure, the only accelerated exposure to combine water and light stressors. No changes in YI of ITO were observed.

Finally, the resistivity of AZO was observed to increase by 250% in the damp heat exposure, shown in Fig. 6, and the AZO resistivity appears to trend upward during the cyclic exposure. The 5 suns UV exposure had no effect on the resistivity of either ITO or AZO. The ITO resistivity was $57 \pm 7\ \Omega/\text{sq}$ for up to 1000 h of damp heat and cyclic exposure.

3.2. Encapsulated PEDOT:PSS Configuration

The previous section explored the results of exposing open-faced TCOs to three accelerated testing protocols. By adding a layer of PEDOT:PSS and encapsulating the sample, a pseudo-cell structure is achieved that mimics an in situ environment. Note that the

PEDOT:PSS was removed and the TCO was cleaned after the exposure, and before the sample characterization; thus measurements of the optical and electrical properties are of the TCO, not of the PEDOT:PSS thin film. The optical properties of the ITO were not affected by the addition of PEDOT:PSS, under any of the accelerated exposure conditions. Qualitatively surveying this configuration, Fig. 7 shows images of AZO where PEDOT:PSS was deposited and immediately removed, subjected to no environmental exposure. The large bulbous hazy area is the initial deposition area where the PEDOT:PSS solution puddle sat for approximately 2–5 s before the spin coating process was initiated. All AZO samples with PEDOT:PSS demonstrated visually similar deposition effects; these effects were not observed for the ITO samples after exposure to PEDOT:PSS.

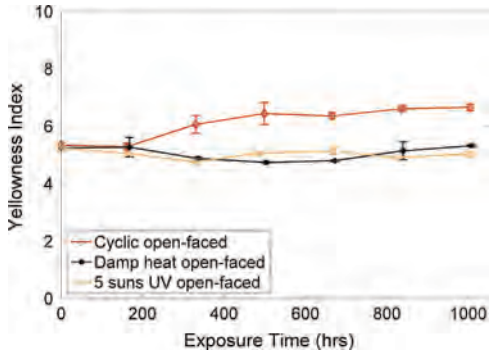

Fig. 5. YI of AZO in the three accelerated exposures, damp heat, cyclic and 5 suns UV.

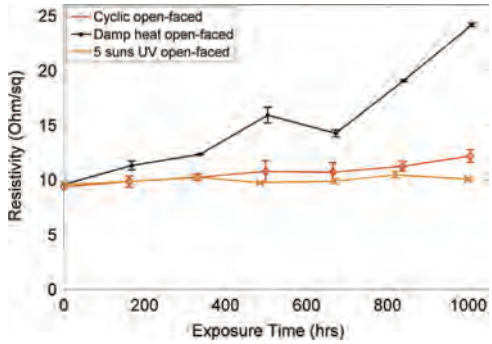

Fig. 6. Resistivity of AZO in the three accelerated exposures, damp heat, cyclic and 5 suns UV.

As with the bare AZO, the interference fringes of the transmission measurements of AZO coated with PEDOT:PSS change with different exposures, as shown in Fig. 8. Here, the additional stressor of the corrosive PEDOT:PSS results in changes in transmission above and beyond those observed for the bare AZO. Both exposures result in a reduction in peak-trough height and rolling of the fringes; additionally, an overall reduction in transmission is observed, greatest in the 5 × outdoor exposure. The reduction in transmission is consistent with the haziness shown in Fig. 7.

For samples exposed with PEDOT:PSS, Fig. 9 shows the %haze, water contact angle and YI data for AZO in both accelerated and real world exposures; open-faced accelerated exposure data for bare AZO are also plotted for comparison. All exposures with PEDOT:PSS are high in haze (greater than 4%) with a large amount of scatter and no trending. The haze is created by application of PEDOT:PSS to the AZO, as shown in Fig. 7; variations in the initial contact time before spincoating may account for the scatter in the haze measurements. The exposure types do not appear to increase the sample haze. Similarly, all exposures with PEDOT:PSS maintain a lower water contact angle than those without. Additionally, the YI of exposures with PEDOT:PSS show a step increase after the initial exposure step (baselines had PEDOT:PSS applied and immediately removed for haze and yellowness measurements).

Finally, a side note about the PEDOT:PSS; a change in hydrophilicity of the PEDOT:PSS was observed after 5 × outdoor exposure. PEDOT:PSS is a mixture of hydrophillic PSS and hydrophobic PEDOT; the freshly deposited material is hydrophillic. After the ITO/PEDOT:PSS samples were subjected to the 5 × outdoor exposure, a portion of the polymer became hydrophobic. Fig. 10 shows that the hexagonal area in the center is hydrophobic (86° water contact angle), whereas the surrounding area is hydrophillic (26° water contact angle). The central hexagonal area is consistent with the shape of the front surface mirror that concentrates light onto the sample, suggesting a light induced polymer rearrangement/degradation.

3.3. Silane protective layer on open-faced TCO

Organofunctional silanes are proposed as a possible protective layer for TCOs. When APTES was applied to AZO, a significant improvement over bare TCO degradation was seen in both the physical and electrical properties. In Fig. 11, micrograph images of the edges of AZO samples show (a) a shelf aged sample, (b) damp heat exposed AZO, and two areas (c,d) of AZO with silane exposed to damp heat. Without a silane protective layer, the 5 cm square sample had a ~ 2 mm wide swath of pitting and delamination edge effects around the entire sample perimeter. With the silane protective layer, these edge effects were almost entirely

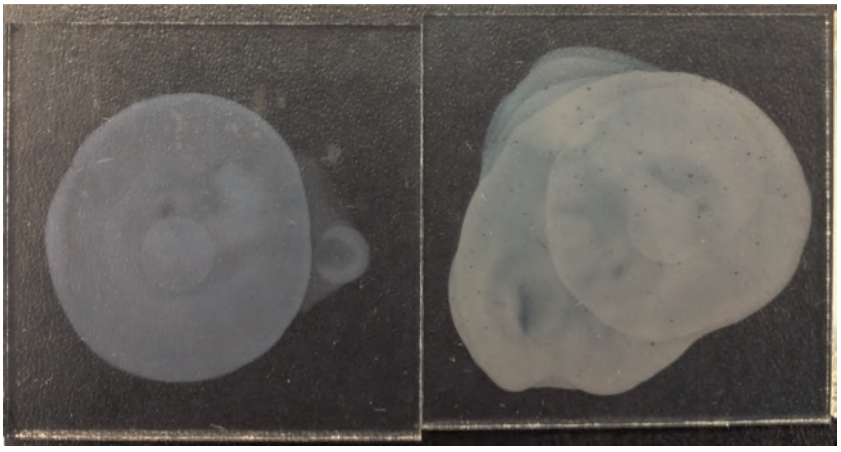

Fig. 7. Images of two AZO samples with PEDOT:PSS deposited and immediately removed.

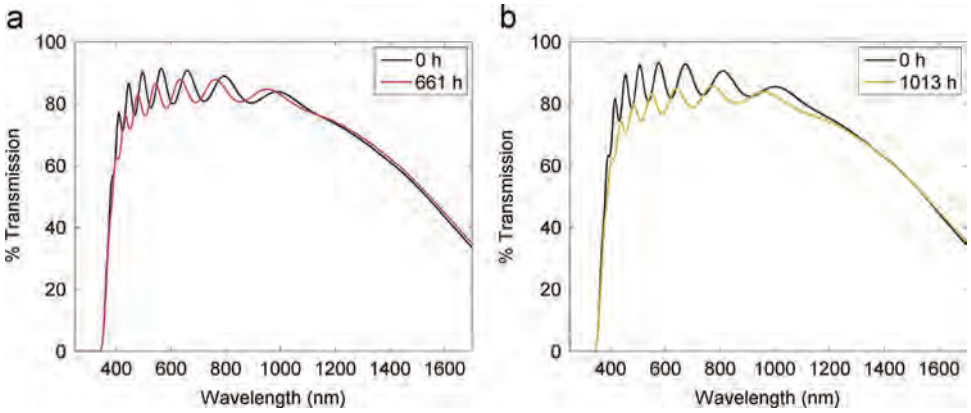

Fig. 8. The % transmission spectrum of AZO from 200 nm to 1800 nm, (a) damp heat encapsulated with PEDOT:PSS, and (b) 5 × outdoor encapsulated with PEDOT:PSS exposures, qualitatively demonstrating increased degradation with addition of a light stressor.

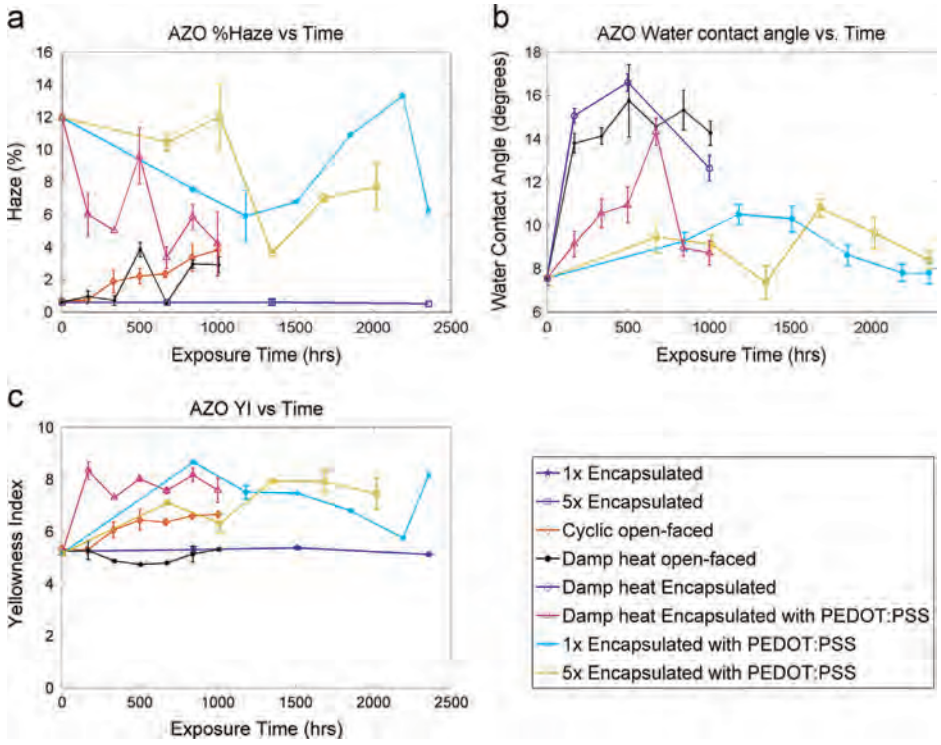

Fig. 9. AZO (a) haze, (b) water contact angle and (c) YI in various exposures with PEDOT:PSS, demonstrating a high, variable haze, a lower water contact angle than bare TCOs, and a step increase in YI at the first time step. Baselines had PEDOT:PSS applied and immediately removed for haze and yellowness measurements. Baseline water contact angles are on bare AZO.

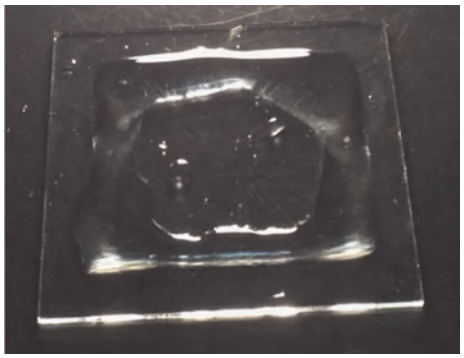

Fig. 10. This image shows water clinging to an ITO/PEDOT:PSS stack after 5 × outdoor exposure, demonstrating hydrophobicity in the region of exposure.

eliminated, reducing the area and extent of the degradation to only a few locations around the perimeter, <1 mm wide.

Degradation of the electrical properties of the AZO by damp heat exposure is also mitigated by the application of the silane layer. Exposure of bare AZO to 1000 h of damp heat resulted in a 250 % increase in resistivity; the addition of the APTES layer reduced the value to only a 60% increase, Fig. 12.

4. Discussion

4.1. Degradation with interfacial layers

Two surface modifications were applied to AZO and ITO, PEDOT:PSS and a silane (APTES), to observe the degradation of the

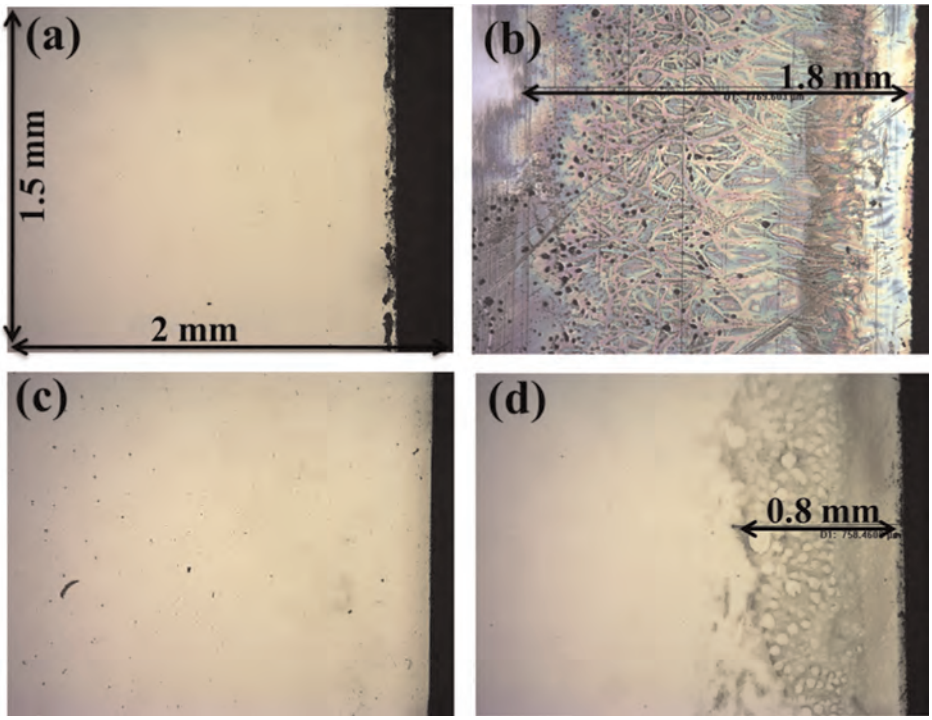

Fig. 11. Micrograph images of the edges of AZO samples that were (a) unexposed, (b) exposed to 1000 h of damp heat, (c) exposed to 1000 h of damp heat with APTES layer showing no degradation, (d) exposed to 1000 h of damp heat exposure with APTES layer showing some degradation.

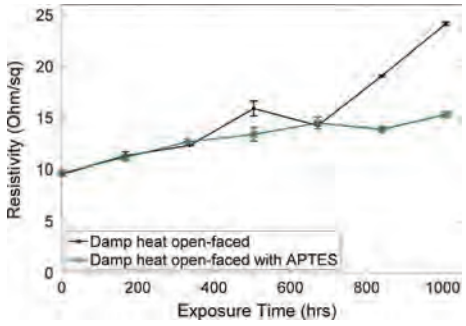

Fig. 12. Resistivity of AZO with and without silane exposed to damp heat. Without the silane protective layer, a resistivity increase of 250% is observed, while the silane-protected AZO resistivity only increases by 60%.

TCO in the context of a device. ITO properties were observed to be stable with both PEDOT:PSS and APTES layers within statistical significance. AZO served as the canary in a coal mine. Firstly, the images in Fig. 7 clearly demonstrate that the majority of the optical degradation due to the PEDOT:PSS stressor on AZO occurs at deposition. This is consistent with PEDOT:PSS literature [14,62], and agrees with the known sensitivity of AZO to acidic aqueous conditions; the PEDOT:PSS solution is water based, so the deposition involves the highest level of water exposure in combination with an acidic environment. AZO haze data (Fig. 9a) support that degradation occurs at deposition; the baseline is high, and the data are scattered and do not trend with exposure time. Secondly, combining the PEDOT:PSS stressor with environmental stressors resulted in decreased water contact angles (Fig. 9), implying a roughening of the AZO surface. This is borne out in the changes in AZO transmission spectra in Figs. 3 and 8. These PEDOT:PSS exposed samples also demonstrate the highest YI observed in all exposures conducted; YI after approximately 100 h is universally high and does not trend with time. For perspective, simply applying a PEDOT:PSS layer to AZO causes the same optical degradation as 1000 h of cyclic exposure of the bare AZO.

Clearly, PEDOT:PSS is not a compatible surface modifier for AZO. In contrast, the application of APTES, an organofunctional silane and known water-resistant surface modifier [24,32,33,14], was found to be beneficial to AZO. From the optical images in Fig. 11, it is clear that the application of the silane has reduced the occurrence and extent of the edge delamination-type degradation in AZO due to a humidity stressor. The silane layer also protects the electrical properties of the AZO film, reducing the resistivity increase from 250% to only 60% after 1000 h of damp heat exposure. These are promising results for incorporation into a device: appropriate choice of a surface modifier can both offer protection of critical underlying material properties and customize the TCO by selection of the silane functionality. The next step in testing silane protection for TCOs is to expose a TCO+silane stack in an encapsulated configuration to a multifactor environmental exposure. These results for both the PEDOT:PSS and silane systems demonstrate the importance of testing materials in context; degradation modes are added or changed with the addition of device layers.

4.2. *Utility of single and multi-factor exposures*

To deconvolve the degradation modes of a system, the individual components should also be evaluated separately; here we examine the degradation of bare TCOs and put the findings in the larger context of lifetime and degradation science. Observational results, such as spectral changes, can direct further testing to identify specific mechanisms. Comparison of the changes in the AZO spectra under different stressor combinations, Fig. 3, yield qualitative insights into the degradation: as additional stressors are added (humidity and irradiance), additional degradation modes are activated. As such, we now examine statistically robust, quantitative data to better relate stressors, both single and multi-factor, to their mechanistic responses.

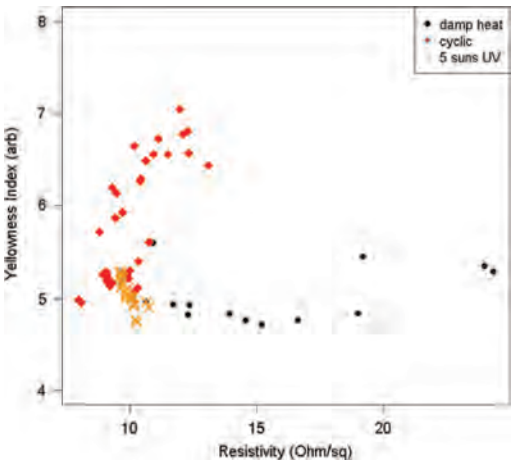

Fig. 13. YI as a function of resistivity of AZO in the three accelerated exposures, damp heat, cyclic and 5 suns UV. This plot combines the results of 3 others into a single image, readily displaying a trade-off between material properties and the activation of different degradation mechanisms.

The examination of water contact angles relates thin film changes seen in spectra to delamination problems observed in deployed technologies. The profound surface sensitivity of TCOs can be observed in the effect of cleaning methods [58]. As observed in Section 3.1, humidity and irradiance stressors each cause a deviation from the baseline water contact angle, but these stressors negate each other when combined (cyclic exposure). This sensitivity to the water:light proportion of the exposure clearly demonstrates the importance of multifactor testing.

Similarly, the YI of AZO increases only in the multifactor cyclic exposure (Fig. 5), suggesting that a new degradation mode indicated by yellowing was activated by the presence of both humidity and irradiance. This also exemplifies the need for simultaneous or sequential multifactor testing.

This is not to say that single stressor testing has no place in lifetime and degradation science research. In Fig. 6, a resistivity increase is observed in all exposures with water as a stressor; a slight increase in cyclic's mild humidity exposure and a drastic increase in damp heat's aggressive humidity environment, reinforcing that the resistivity of AZO is water sensitive [23,63,12,6]. While the damp heat exposure may be an unreasonable acceleration or unrelated to real world degradation mechanisms, this single stressor environment yields a useful response magnitude, enabling deconvolution of multi-stressor testing; a tool to be used in combination with other exposures.

4.2.1. *Mechanistic plot analysis*

Another critical tool for lifetime and degradation science is the variable–variable mechanistic plot, in which two system responses are plotted against each other for different exposure conditions to identify the most realistic multifunction exposures for accelerated screening tests. TCOs have two critical properties to their functionality; conductivity and transparency. Plotting these two variables against one another highlights material property trade-offs, and can reveal insights into the mechanisms of degradation. Fig. 13 plots the YI of AZO versus its resistivity for the different open-faced accelerated exposures.

In this mechanistic plot, we observe as we did previously, that there is no response due to irradiance alone, a large increase in resistivity due to the humidity stressor, and an increase in YI only in the multi-stressor cyclic exposure, accompanied by a slight increase in resistivity. This plot not only combines several plots into one, but clearly displays the different degradation mechanisms activated by different stressor combinations; the YI increase is unrelated to the resistivity increase and both mechanisms can coexist [37]. Mechanistic plots such as these, paired with correlations and statistical models, can lead to the characterization of complex degradation mechanisms and pathways in materials, components and systems [35].

5. Conclusions

A lifetime and degradation science approach was applied to the engineering challenge of TCO degradation in long service-life devices, such as photovoltaics. This data science approach utilized commercially available TCO materials, and subjected them to an array of stressor combinations, including environmental and material stressors. Optical, electrical and surface sensitive TCO metrics were monitored and analyzed in a statistically robust fashion, broadly observing critical macroscopic material properties. From this wide survey, mechanistically different degradation was observed when stressors were combined; PEDOT:PSS application results in hazing and roughening of AZO, while silane coated AZO displayed fewer edge effects and slowed the degradation of the conductivity in damp heat; TCO surfaces are sensitive to the proportion of water and light in an exposure, and the combination of water and UV light is required to activate a yellowing mechanism in AZO. By plotting critical material properties against one another, a mechanistic plot, we observe the trade-offs between properties and the activation of different degradation mechanisms and pathways due to different stressor combinations. Specifically, the YI increase and resistivity increase in AZO are unrelated but can coexist. Through examination of many stressor combinations (both accelerated and real time) critical stressors can be convolved, deconvolved, and applied in realistic proportions to build more accurate degradation pathways, yielding better lifetime predictions and identifying actions to improve lifetime performance.

Acknowledgments

The authors acknowledge Sam Sprawls for his role in silane depositions, and to Lori Postak and the Quanex team for their help with encapsulation design. The authors would also like to acknowledge the funding for this work; the open-faced study was supported by Underwriters Laboratories. The encapsulated study was supported by the Bay Area Photovoltaic Consortium Prime Award no. DE-EE0004946, Subaward Agreement no. 60220829-51077-T. Research was performed at the SDLE Center, which was established through funding through the Ohio Third Frontier, Wright Project Program Award tech 12-004, and at the MORE Center at Case Western Reserve University.

References

[1] B. Roth, G.A. dos Reis Benatto, M. Corazza, R.R. Søndergaard, S.A. Gevorgyan, M. Jørgensen, F.C. Krebs, The critical choice of PEDOT:PSS additives for long term stability of roll-to-roll processed OPVs, Adv. Energy Mater. 5 (9) (2015) 1401912–1401920.

[2] F.C. Krebs, S.A. Gevorgyan, J. Alstrup, A roll-to-roll process to flexible polymer solar cells: model studies, manufacture and operational stability studies, J. Mater. Chem. 19 (30) (2009) 5442–5451.

[3] Y. Ahn, Y. Jeong, Y. Lee, Improved thermal oxidation stability of solution-processable silver nanowire transparent electrode by reduced graphene oxide, ACS Appl. Mater. Interfaces 4 (12) (2012) 6410–6414.

[4] K. Zilberberg, F. Gasse, R. Pagui, A. Polywka, A. Behrendt, S. Trost, R. Heiderhoff, P. Görrn, T. Riedl, Highly robust indium-free transparent conductive electrodes based on composites of silver nanowires and conductive metal oxides, Adv. Funct. Mater. 24 (12) (2014) 1671–1678.

[5] T.J. McMahon, Accelerated testing and failure of thin-film PV modules, Prog. Photovoltaics: Res. Appl. 12 (2–3) (2004) 235–248 , URL ⟨http://onlinelibrary.wiley.com/doi/10.1002/pip.526/abstract⟩.

[6] F.J. Pern, R. Noufi, B. To, C. DeHart, X. Li, S.H. Glick, Degradation of ZnO-based window layers for thin-film CIGS by accelerated stress exposures, Proc. SPIE 7048, Reliability of Photovoltaic Cells, Modules, Components, and Systems, San Diego, 2008, pp. 70480P–70480P-14. http://dx.doi.org/10.1117/12.795097. URL ⟨http://proceedings.spiedigitallibrary.org/proceeding.aspx?articleid=793618⟩.

[7] R. Feist, S. Rozeveld, B. Kern, J. D'Archangel, S. Yeung, M. Bernius, Further investigation of the lifetime-limiting failure mechanisms of CIGSS-based minimodules under environmental stress, in: 2009 34th IEEE Photovoltaic Specialists Conference (PVSC), 2009, pp. 002359–002363. URL ⟨http://ieeexplore.ieee.org/xpls/abs_all.jsp?arnumber=5411323⟩.

[8] M. Jorgensen, K. Norrman, F.C. Krebs, Stability/degradation of polymer solar cells, Solar Energy Mater. Solar Cells 92 (7) (2008) 686–714, http://dx.doi.org/10.1016/j.solmat.2008.01.005, URL ⟨http://linkinghub.elsevier.com/retrieve/pii/S0927024808000056⟩.

[9] C.R. Osterwald, T.J. McMahon, J.A. del Cueto, J. Adelstein, J. Pruett, Accelerated stress testing of thin-film modules with SnO_2: f transparent conductors, in: National Center for Photovoltaics and Solar Program Review Meeting Denver, Colorado March, 2003, pp. 24–26. URL ⟨http://www.nrel.gov/docs/fy03osti/33567.pdf⟩.

[10] K.W. Jansen, A. Varvar, E. Twesme, T. Berens, N.G. Dhere, Design of high-reliability low-cost amorphous silicon modules for high energy yield, in: Solar Energy+Applications, 2008, p. 70480M. URL ⟨http://proceedings.spiedigitallibrary.org/proceeding.aspx?articleid=1338222⟩.

[11] W. Beyer, J. Hupkes, H. Stiebig, Transparent conducting oxide films for thin film silicon photovoltaics, Thin Solid Films 516 (2–4) (2007) 147–154, http://dx.doi.org/10.1016/j.tsf.2007.08.110, URL ⟨http://linkinghub.elsevier.com/retrieve/pii/S004060900701512X⟩.

[12] R. Sundaramoorthy, F.J. Pern, C. DeHart, T. Gennett, F.Y. Meng, M. Contreras, T. Gessert, Stability of TCO window layers for thin-film CIGS solar cells upon damp heat exposures: part II, in: SPIE Solar Energy+Technology, 2009, 74120J-1–74120J-12. URL ⟨http://proceedings.spiedigitallibrary.org/proceeding.aspx?articleid=1340457⟩.

[13] M.D. Kempe, K.M. Terwilliger, D. Tarrant, Stress induced degradation modes in cigs mini-modules, in: 33rd IEEE Photovoltaic Specialists Conference, San Diego, 2008, IEEE, pp. 1–6.

[14] K.W. Wong, H.L. Yip, Y. Luo, K.Y. Wong, W.M. Lau, K.H. Low, H.F. Chow, Z. Q. Gao, W.L. Yeung, C.C. Chang, Blocking reactions between indium-tin oxide and poly (3,4-ethylene dioxythiophene):poly(styrene sulphonate) with a self-assembly monolayer, Appl. Phys. Lett. 80 (15) (2002) 2788, http://dx.doi.org/10.1063/1.1469220, URL ⟨http://link.aip.org/link/APPLAB/v80/i15/p2788/s1&Agg=doi⟩.

[15] M.P. De Jong, L.J. Van Ijzendoorn, M.J.A. De Voigt, Stability of the interface between indium-tin-oxide and poly (3, 4-ethylenedioxythiophene)/poly (styrenesulfonate) in polymer light-emitting diodes, Appl. Phys. Lett. 77 (14) (2000) 2255–2257 , URL ⟨http://ieeexplore.ieee.org/xpls/abs_all.jsp?arnumber=4904664⟩.

[16] M. Girtan, M. Rusu, Role of ITO and PEDOT: PSS in stability/degradation of polymer:fullerene bulk heterojunctions solar cells, Solar Energy Mater. Solar Cells 94 (3) (2010) 446–450, http://dx.doi.org/10.1016/j.solmat.2009.10.026, URL ⟨http://linkinghub.elsevier.com/retrieve/pii/S092702480900381X⟩.

[17] N. Grossiord, J.M. Kroon, R. Andriessen, P.W. Blom, Degradation mechanisms in organic photovoltaic devices, Org. Electron. 13 (3) (2012) 432–456, http://dx.doi.org/10.1016/j.orgel.2011.11.027, URL ⟨http://linkinghub.elsevier.com/retrieve/pii/S1566119911004046⟩.

[18] N.R. Armstrong, P.A. Veneman, E. Ratcliff, D. Placencia, M. Brumbach, Oxide contacts in organic photovoltaics: characterization and control of near-surface composition in Indium-Tin oxide (ITO) electrodes, Accounts Chem. Res. 42 (11) (2009) 1748–1757, http://dx.doi.org/10.1021/ar900096f, URL ⟨http://pubs.acs.org/doi/abs/10.1021/ar900096f⟩.

[19] A.W. Hains, C. Ramanan, M.D. Irwin, J. Liu, M.R. Wasielewski, T.J. Marks, Designed bithiophene-based interfacial layer for high-efficiency bulk-heterojunction organic photovoltaic cells. importance of interfacial energy level matching, ACS Appl. Mater. Interfaces 2 (1) (2009) 175–185.

[20] W. Leung, Y. Chan, S. Lui, A study of degradation of indium tin oxide thin films on glass for display applications, Microelectron. Eng. 101 (2013) 1–7, http://dx.doi.org/10.1016/j.mee.2012.08.002, URL ⟨http://linkinghub.elsevier.com/retrieve/pii/S0167931712004352⟩.

[21] F.J. Pern, R. Noufi, B. To, C. DeHart, X. Li, S.H. Glick, Degradation of ZnO-based window layers for thin-film CIGS by accelerated stress exposures, Solar Energy+Applications, International Society for Optics and Photonics, 2008, p. 70480P, http://dx.doi.org/10.1117/12.795097.

[22] D. Greiner, S. Gledhill, C. Koble, J. Krammer, R. Klenk, Damp heat stability of Al-doped zinc oxide films on smooth and rough substrates, Thin Solid Films 520 (4) (2011) 1285–1290, http://dx.doi.org/10.1016/j.tsf.2011.04.190, URL ⟨http://linkinghub.elsevier.com/retrieve/pii/S0040609011010315⟩.

[23] T. Tohsophon, J. Hupkes, S. Calnan, W. Reetz, B. Rech, W. Beyer, N. Sirikulrat, Damp heat stability and annealing behavior of aluminum doped zinc oxide films prepared by magnetron sputtering, Thin Solid Films 511–512 (2006) 673–677, http://dx.doi.org/10.1016/j.tsf.2005.12.130, URL ⟨http://linkinghub.elsevier.com/retrieve/pii/S0040609005024685⟩.

[24] M. Brumbach, N.R. Armstrong, Encyclopedia of Electrochemistry: Modification of Transparent Conducting Oxide (TCO) Electrodes through Silanization and Chemisorption of Small Molecules, Wiley-VCH, Weinheim, 2007.

[25] C.K. Song, A.C. White, L. Zeng, B.J. Leever, M.D. Clark, J.D. Emery, S.J. Lou, A. Timalsina, L.X. Chen, M.J. Bedzyk, et al., Systematic investigation of organic photovoltaic cell charge injection/performance modulation by dipolar organosilane interfacial layers, ACS Appl. Mater. Interfaces 5 (18) (2013) 9224–9240.

[26] H.M. Lemire, K.A. Peterson, M.S. Breslau, K.D. Singer, I.T. Martin, R.H. French, Degradation of transparent conductive oxides, and the beneficial role of interfacial layers, MRS Online Proc. Libr. (2013), http://dx.doi.org/10.1557/opl.2013.695, mrss13–1537.

[27] H.M. Lemire, K.A. Peterson, S. Sprawls, K. Singer, I.T. Martin, R.H. French, Degradation of transparent conductive oxides: mechanistic insights across configurations and exposures, in: SPIE Solar Energy+Technology, International Society for Optics and Photonics, San Diego, 2013, p. 882502. http://dx.doi.org/10.1117/12.2024691.

[28] C.G. Allen, D.J. Baker, J.M. Albin, H.E. Oertli, D.T. Gillaspie, D.C. Olson, T.E. Furtak, R.T. Collins, Surface modification of ZnO using triethoxysilane-based molecules, Langmuir 24 (23) (2008) 13393–13398, http://dx.doi.org/10.1021/la802621n, URL ⟨http://pubs.acs.org/doi/abs/10.1021/la802621n⟩.

[29] M.O. Reese, A.J. Morfa, M.S. White, N. Kopidakis, S.E. Shaheen, G. Rumbles, D.S. Ginley, Pathways for the degradation of organic photovoltaic P3HT: PCBM based devices, Solar Energy Mater. Solar Cells 92 (7) (2008) 746–752, http://dx.doi.org/10.1016/j.solmat.2008.01.020, URL ⟨http://linkinghub.elsevier.com/retrieve/pii/S0927024808000305⟩.

[30] R.A. Shircliff, P. Stradins, H. Moutinho, J. Fennell, M.L. Ghirardi, S.W. Cowley, H.M. Branz, I.T. Martin, Angle-resolved xps analysis and characterization of monolayer and multilayer silane films for dna coupling to silica, Langmuir 29 (12) (2013) 4057–4067, http://dx.doi.org/10.1021/la304719y, URL ⟨http://pubs.acs.org/doi/pdf/10.1021/la304719y⟩.

[31] X. Guo, T.J. Marks, Plastic solar cells with engineered interfaces, in: SPIE OPTO, International Society for Optics and Photonics, San Diego, 2013, p. 86220K.

[32] C.-K. Chien, Application of silane-enhanced adhesion promoters for optical fibers and fiber ribbons, US Patent 6,577,802, June 10, 2003.

[33] P.G. Pape, E.P. Plueddemann, Methods for improving the performance of silane coupling agents, J. Adhes. Sci. Technol. 5 (10) (1991) 831–842 , URL ⟨http://www.tandfonline.com/doi/abs/10.1163/156856191X00242⟩.

[34] M.P. Murray, L.S. Bruckman, R.H. French, Photodegradation in a stress and response framework: poly(methyl methacrylate) for solar mirrors and lens, J. Photonics Energy 2 (1) (2012), http://dx.doi.org/10.1117/1.JPE.2.022004 022004–022004.

[35] L.S. Bruckman, N.R. Wheeler, J. Ma, E. Wang, C.K. Wang, I. Chou, J. Sun, R.H. French. Statistical and Domain Analytics Applied to PV Module Lifetime and Degradation Science. IEEE Access 1 (2013): 384-403. http://dx.doi.org/10.1109/ACCESS.2013.2267611.

[36] Hossain, Mohammad Akram, Yifan Xu, Timothy J. Peshek, Liang Ji, Alexis R. Abramson, and Roger H. French. "Microinverter Thermal Performance in the Real-World: Measurements and Modeling." PLoS ONE 10, no. 7 (July 6, 2015): e0131279. http://dx.doi.org/10.1371/journal.pone.0131279.

[37] R.H. French, R. Podgornik, T.J. Peshek, L.S. Bruckman, Y. Xu, N.R. Wheeler, A. Gok, Y. Hu, M.A. Hossain, D.A. Gordon, Degradation science: Mesoscopic evolution and temporal analytics of photovoltaic energy materials, Current Opin. Solid State Mater. Sci. 19 (4) (2015) 212–226, http://dx.doi.org/10.1016/j.cossms.2014.12.008.

[38] L.S. Bruckman, N.R. Wheeler, I.V. Kidd, J. Sun, and R.H. French. Photovoltaic Lifetime & Degradation Science Statistical Pathway Development: Acrylic Degradation. In Reliability of Photovoltaic Cells, Modules, Components, and Systems VI, Vol. 8825. Bellingham: Spie-Int Soc. Optical Engineering, 2013, http://dx.doi.org/10.1117/12.2024717.

[39] Y. Hu, M.A. Hosain, T. Jain, Y.R. Gunapati, L. Elkin, G. Zhang, R.H. French, Global sunfarm data acquisition network, energy cradle, and time series analysis, in: Energytech, 2013 IEEE, Cleveland, pp. 1–5. http://dx.doi.org/10.1109/EnergyTech.2013.6645317.

[40] M.A. Hossain, T.J. Peshek, Y. Xu, L. Ji, J. Sun, A. Abramson, R.H. French, Thermal performance of microinverters on dual-axis trackers, in: SPIE Solar Energy+Technology, International Society for Optics and Photonics, 2014, p. 91790J. http://dx.doi.org/10.1117/12.2061235.

[41] L.S. Bruckman, M.P. Murray, S. Richardson, S.A. Brown, M. Schuetz, R. French, Degradation of back surface acrylic mirrors: implications for low concentration and mirror augmented photovoltaics, in: Energytech, 2012 IEEE, Cleveland, pp. 1–4. http://dx.doi.org/10.1109/EnergyTech.2012.6304678.

[42] C.R. Osterwald, T.J. McMahon, History of accelerated and qualification testing of terrestrial photovoltaic modules: a literature review, Prog. Photovoltaics: Res. Appl. 17 (1) (2009) 11–33, http://dx.doi.org/10.1002/pip.861, URL ⟨http://doi.wiley.com/10.1002/pip.861⟩.

[43] T.J. McMahon, G.J. Jorgensen, R.L. Hulstrom, D.L. King, M.A. Quintana, Module 30 year life: what does it mean and is it predictable/achievable?, in: Program and Proceedings: NCPV Program Review Meeting 2000, NREL,, pp. 17–18.

[44] F. Pern, R. Noufi, X. Li, C. DeHart, B. To, Damp-heat induced degradation of transparent conducting oxides for thin-film solar cells, in: 33rd IEEE Photovoltaic Specialists Conference, PVSC'08 San Diego, 2008, pp. 1–6.

[45] S. Boslaugh, Statistics in a Nutshell, O'Reilly Media, Inc., Sebastopol, 2012.

[46] A.E. Delahoy, S. Guo, Transparent Conducting Oxides for Photovoltaics, John Wiley and Sons, Ltd., Chichester, UK, 2011, pp. 716–796. http://dx.doi.org/10.1002/9780470974704.ch17.

[47] D.C. Ince, L. Hatton, J. Graham-Cumming, The case for open computer programs, Nature 482 (7386) (2012) 485–488, http://dx.doi.org/10.1038/

nature10836, URL ⟨http://www.nature.com/nature/journal/v482/n7386/full/nature10836.html⟩.
[48] Open Data Charter. URL ⟨https://www.gov.uk/government/publications/open-data-charter⟩, June 2013.
[49] J. Andraka, US open access: The Pathway to Innovation. URL ⟨http://www.whitehouse.gov/blog/2013/06/20/open-access-pathway-innovation⟩, 2013.
[50] B. Obama, US OSTP Executive Order—Making Open and Machine Readable the New Default for Government Information | the White House. URL ⟨http://www.whitehouse.gov/the-press-office/2013/05/09/executive-order-making-open-and-machine-readable-new-default-government-⟩, 2013.
[51] R. Cotton, Learning R: A Step-by-Step Function Guide to Data Analysis, O'Reilly Media, Inc., Sebastapool, 2011. URL ⟨http://shop.oreilly.com/product/0636920028352.do⟩.
[52] P.K. Janert, Data Analysis with Open Source Tools: A Hands-on Guide for Programmers and Data Scientists. O'Reilly Media, Inc., Sebastapool, 2010. URL ⟨http://shop.oreilly.com/product/9780596802363.do⟩.
[53] T.R. Project, F.S. Foundation, The R Foundation for Statistical Computing. URL ⟨http://www.r-project.org/index.html⟩, October 2014.
[54] P. Teetor, R Cookbook, O'Reilly Media, Inc., Sebastopol, 2011.
[55] N. Matloff, The Art of R Programming: a Tour of Statistical Software Design, No Starch Press, San Francisco, 2011.
[56] P. Teetor, 25 Recipes for Getting Started with R, O'Reilly Media, Inc., Sebastopol, 2011.
[57] H.M. Lemire, Degradation of transparent conductive oxides: Mechanistic insights and interfacial engineering (Master's thesis), Case Western Reserve University. URL ⟨http://rave.ohiolink.edu/etdc/view?acc_num=case1386325661⟩, 2014.
[58] M.D. Clark, B.J. Leever, Analysis of ITO cleaning protocol on surface properties and polymer: fullerene bulk heterojunction solar cell performance, Solar Energy Mater. Solar Cells 116 (2013) 270–274, http://dx.doi.org/10.1016/j.solmat.2013.05.010, URL ⟨http://linkinghub.elsevier.com/retrieve/pii/S0927024813002195⟩.
[59] M.P. Murray, Development and optimization of back surface acrylic solar mirrors to assure 25 year lifetime performance (Master's thesis), Case Western Reserve University. URL ⟨http://rave.ohiolink.edu/etdc/view?acc_num=case1364987929⟩, 2012.
[60] M.D. Kempe, D. Panchagade, M.O. Reese, A.A. Dameron, Modeling moisture ingress through polyisobutylene-based edge-seals, Prog. Photovoltaics: Res. Appl. 23 (5) (2015) 570–581.
[61] J.A. Howarter, J.P. Youngblood, Optimization of silica silanization by 3-aminopropyltriethoxysilane, Langmuir 22 (26) (2006) 11142–11147.
[62] K. Kawano, R. Pacios, D. Poplavskyy, J. Nelson, D.D. Bradley, J.R. Durrant, Degradation of organic solar cells due to air exposure, Solar Energy Mater. Solar Cells 90 (20) (2006) 3520–3530, http://dx.doi.org/10.1016/j.solmat.2006.06.041, URL ⟨http://linkinghub.elsevier.com/retrieve/pii/S0927024806002960⟩.
[63] R. Sundaramoorthy, F.J. Pern, G. Teeter, J.V. Li, M. Young, D. Kuciauskas, B. To, F. Yan, S. Johnston, R. Noufi, Influence of damp heat on the electrical, optical, and morphological properties of encapsulated CuInGaSe2 devices, in: Proceedings of 37 IEEE PVSC. URL ⟨http://www.nrel.gov/docs/fy11osti/50841.pdf⟩.